nature plants

Supplementary information https://doi.org/10.1038/s41477-024-01846-1

Evidence for widespread thermal acclimation of canopy photosynthesis

In the format provided by the authors and unedited

Evidence for widespread thermal acclimation of canopy photosynthesis

Jiangong Liu[1*], Youngryel Ryu[1,2*], Xiangzhong Luo[3], Benjamin Dechant[1,4,5], Benjamin D. Stocker[6,7], Trevor F. Keenan[8,9], Pierre Gentine[10,11], Xing Li[1], Bolun Li[1,12], Sandy P. Harrison[13,14], Iain Colin Prentice[14,15]

[1] Research Institute of Agriculture and Life Sciences, Seoul National University, Seoul, Republic of Korea
[2] Department of Landscape Architecture and Rural Systems Engineering, Seoul National University, Seoul, Republic of Korea
[3] Department of Geography, National University of Singapore, 1 Arts Link, Singapore 117570
[4] German Centre for Integrative Biodiversity Research (iDiv) Halle-Jena-Leipzig, Leipzig, Germany
[5] Leipzig University, Leipzig, Germany
[6] Institute of Geography, University of Bern, Bern, Switzerland
[7] Oeschger Centre for Climate Change Research, University of Bern, Bern, Switzerland
[8] Climate and Ecosystem Sciences Division, Lawrence Berkeley National Laboratory, 1 Cyclotron Road, Berkeley, CA 94720, USA
[9] Department of Environmental Science, Policy, and Management, University of California, Berkeley, CA 94720, USA
[10] Earth and Environmental Engineering Department, Columbia University, New York, NY 10027, USA
[11] Climate School, Columbia University, New York, NY 10025, USA
[12] School of Geographical Sciences, Nanjing University of Information Science and Technology, Nanjing 210044, China
[13] School of Archaeology, Geography and Environmental Science (SAGES), University of Reading, Reading RG6 6AH, United Kingdom
[14] Department of Earth System Science, Ministry of Education Key Laboratory for Earth System Modeling, Institute for Global Change Studies, Tsinghua University, Beijing 100084, China
[15] Georgina Mace Centre for the Living Planet, Department of Life Sciences, Imperial College London, Silwood Park Campus, Buckhurst Road, Ascot SL5 7PY, United Kingdom

*Corresponding author: Jiangong Liu (jl6314@columbia.edu); Youngryel Ryu (yryu@snu.ac.kr)

The SI contains 2 Supplementary Text, 3 Supplementary Tables, 9 Supplementary Figures, and Supplementary References.

Supplementary Text 1. Farquhar-von Caemmerer-Berry model (FvCB) for estimating CO_2 assimilation rate

We employ the standard FvCB model[1], which comprises the photosynthetic module of the Breathing Earth System Simulator (BESS)[2,3], to estimate the canopy-scale CO_2 assimilation rate (A) of C_3 plants in a big-leaf framework. Within the big-leaf framework, we assume the canopy functions as a single bulk plane that serves as the source and sink for all mass and energy fluxes[4]. The model determines A based on the slower rate of two biochemical processes: A_j, which is the electron transport for ribulose-1,5-bisphosphate (RuBP) at low light and is dependent on the capacity of the electron transport chain (J_{max}; μmol m^{-2} s^{-1}), and A_c, which is the carboxylation of RuBP and is dependent on ribulose-1,5-bisphosphate carboxylase/oxygenase (Rubisco) activities (V_{cmax}; μmol m^{-2} s^{-1}). Both A_j and A_c are influenced by intercellular CO_2 concentrations (C_i). For non-optimality-based BESS versions (i.e., $BESS_{PFT}$ and $BESS_{LAI}$), we assume a fixed ratio of C_i to the ambient CO_2 concentration (C_a), which is referred to as χ and set at 0.7[5]. The eco-evolutionary optimality (EEO) theory suggests that plants tend to maximize carbon gain and minimize water loss by regulating stomatal conductance, which results in an optimal χ value[6]. We use optimal χ for optimality-based BESS ($BESS_{EEO}$) (Supplementary Text 2).

$$A_j = \frac{\alpha I J_{max}}{\alpha I + 2.1 J_{max}} \frac{(C_i - \Gamma^*)}{4(C_i + 2\Gamma^*)} \tag{1}$$

$$A_c = \frac{V_{cmax}(C_i - \Gamma^*)}{C_i + K_c\left(1 + \frac{O}{K_o}\right)} \tag{2}$$

$$A = \min(A_c, A_j) \tag{3}$$

where I (μmol photons m^{-2} s^{-1}) is incident photosynthetically photon flux density, α (mol mol^{-1}) is the intrinsic quantum yield based on incident light, Γ^* (Pa) is the CO_2 compensation point in the absence of dark respiration, O (Pa) is oxygen partial pressure, and K_c (Pa) and K_o (Pa) are Michaelis-Menten constants of Rubisco for CO_2 and O_2, respectively[7].

In this study, we integrate the parameters characterizing acclimation and adaptation following ref[8] into the BESS code. An Arrhenius function is used to describe the temperature dependencies of V_{cmax} and J_{max} for the baseline BESS[9]:

$$k = k^{25C} \times \exp\left[\frac{H_a \times 1000 \times (T - 298.15)}{298.15 \times R \times T}\right] \times \frac{\left[1 + \exp\left(\frac{298.15 \times S - H_d}{298.15 \times R}\right)\right]}{\left[1 + \exp\left(\frac{S \times T - H_d}{R \times T}\right)\right]} \quad (4)$$

where k^{25C} represents V_{cmax}^{25C} and J_{max}^{25C}, and R is the universal gas constant (8.31 J K^{-1} mol^{-1}). T is the canopy temperature in °K. H_a, H_d and S are activation energy (kJ mol^{-1}), deactivation energy fixed at 200 kJ mol^{-1}, and entropy factor (kJ mol^{-1} K^{-1}), respectively.

We use three empirical approaches to estimate V_{cmax} variants at a reference temperature of 25 °C (V_{cmax}^{25C}) (see Methods), and calculate J_{max}^{25C} as a function of V_{cmax}^{25C}, home temperature (T_{home}, °C) and growth temperature ($\overline{T_{air}}$, °C)[8]. Here, T_{home} is defined as the average air temperature of the warmest month over the measurement period following ref[10]. The values of H_a and S are estimated as functions of $\overline{T_{air}}$ and T_{home} to account for acclimation, with a general form as:

$$H_a \text{ or } S = a\overline{T_{air}} + bT_{home} + c(\overline{T_{air}} - T_{home}) + d \quad (5)$$

where parameters a, b, c and d are set, following refs[8,10] and can be found in Supplementary Table 2. T represents a key source of uncertainties in canopy-scale photosynthetic modelling[10]. We test three approaches to estimate T, which assume that T is equivalent to either the air temperature (T_{air}, °K), the aerodynamic surface temperature (T_{aero}, °K), or the radiometric surface temperature of the big-leaf plane (T_{rad}, °K). T_{aero} is calculated as follows:

$$T_{aero} = T_{air} + \frac{H}{\rho G_{ah} c_p} \quad (6)$$

where H is the sensible heat flux (W m^{-2}), ρ is the air density (kg m^{-3}), G_{ah} is the aerodynamic conductance to heat transfer (m s^{-1}), and C_p is the heat capacity of dry air (J K^{-1} kg^{-1}). G_{ah} is calculated as the sum of aerodynamic conductance to momentum transfer[11] and canopy boundary layer conductance to heat transfer[12]. T_{rad} is calculated based on the physical principle that the longwave radiation emitted by an object is proportional to the fourth power of the object's temperature, stated by the Stephan-Boltzmann law:

$$T_{rad} = \left(\frac{LW_{out} - (1 - \epsilon)LW_{in}}{\sigma\epsilon}\right)^{\frac{1}{4}} \quad (7)$$

where LW_{out} and LW_{in} are the outgoing and incoming longwave radiation (W m^{-2}), respectively. σ denotes the Stefan-Boltzmann constant (W m^{-2} K^{-4}). We set the emissivity of the surface, ϵ, to 0.98. We compute T_{aero} and T_{rad} with R package bigleaf[4]. Note that the data availability for T_{rad}

and T_{aero} data is less than that for T_{air}, as their calculation depends on several variables (equation 6 and 7). This is particularly significant given that LW_{out} and LW_{in} are available for only about 74% of the sites. The estimated T_{aero} and T_{rad} show strong correlations with T_{air}, with R^2 values of 0.93 ± 0.10 and 0.78 ± 0.15 (mean ± 1–SD, model: T_{air} ~ T_{aero} or T_{rad}) over FLUXNET2015 sites. In theory, T_{rad} and T_{aero} should more closely approximate the true canopy temperature (T) than T_{air}, potentially leading to better model performance when using them as T approximations. However, the three T approximations (i.e., T_{air}, T_{aero} and T_{rad}) yield highly similar results when estimating hourly *A* (Supplementary Fig. 8). It is important to note that eddy covariance GPP data are not independent of T_{air}, since both daytime and nighttime partitioning methods use T_{air} as an input[13]. This likely explains the comparable modelling performance between T_{air} and the other two T approximations. We finally choose T_{air} over T_{aero} and T_{rad} because the data are more frequently available. Detailed descriptions of other processes of the FvCB model in BESS and BESS's performance in estimating GPP over flux sites are given in refs[2,3,9].

Supplementary Text 2. EEO-based estimate of leaf photosynthetic capacity

The coordination hypothesis posits that leaf A_c (equation 2) tends to be equal to A_j (equation 1) over intermediate time scales, meaning that photosynthesis operates at a co-limitation point of A_c and A_j[14,15]. We apply the findings from this study on PFT-dependent optimal time scales for acclimation (Fig. 2) to represent the growth conditions of plants. To account for the effect of finite J_{max}[6,16], we modify equation (1) using a non-rectangular hyperbola function[17]:

$$A_j = \frac{\alpha I}{\sqrt{1 + \left(\frac{\alpha I}{J_{max}}\right)^2}} \frac{(C_i - \Gamma^*)}{(C_i + 2\Gamma^*)} \quad (8)$$

$$\alpha = \frac{a_L b_L}{4} \Phi_{PSII,max} M \quad (9)$$

where a_L = 0.8 represents the leaf absorptance, b_L = 0.5 represents the fraction of absorbed light for photosystem II (PSII), and the factor 4 accounts for the number of electron equivalents required to assimilate one CO_2 molecule. The constant M = 12 (g) represents the weight of 1 mol carbon. $\Phi_{PSII,max}$ represents the maximum quantum yield of PSII for a representative light-adapted leaf, and is dependent on T[18]:

$$\Phi_{PSII,max} = 0.352 + 0.022T - 0.00034T^2 \quad (10)$$

The least-cost theory proposes that plants can optimize χ by minimizing the combined unit costs per carbon assimilation of maintaining carbon assimilation and water transpiration (E)[19]:

$$e\frac{\partial(E/A)}{\partial\chi} = -f\frac{\partial(V_{cmax}/A)}{\partial\chi} \quad (11)$$

where e and f (unitless) are the unit costs for E and A, respectively. One optimal χ value can be resolved from equation (10) through an application of Fick's law of diffusion for H_2O and CO_2[19]:

$$\chi = \frac{\sqrt{\beta\frac{K+\Gamma^*}{1.6\eta^*}} + \frac{\Gamma^*\sqrt{VPD}}{C_a}}{\sqrt{\beta\frac{K+\Gamma^*}{1.6\eta^*}} + \sqrt{VPD}} \quad (12)$$

where VPD (Pa) is the vapor pressure deficit, and K (Pa) is the effective Michaelis-Menten coefficient of Rubisco[20]. η^* (Pa s), which represents the viscosity of water at 25 °C, can be estimated using a T dependence function[6]. The parameter β is the ratio of the unit costs a and b (equation 9) when standardized to their values at 25 °C, and is fixed at 146 based on an updated isotope-derived χ database[6,16].

Furthermore, we assume that the optimal J_{max} value maximizes the difference between carbon gain (A_j) and the cost of c×J_{max}, where c (unitless) is a cost factor. We estimate c to be 0.103 based on a typical value of $J_{max}/V_{cmax} = 1.88$[6,21]. By establishing an equivalence between equations (2) and (7), we can solve for an EEO-based leaf-scale V_{cmax} value (V_{cmax_EEO}):

$$V_{cmax\_EEO} = \alpha I\frac{C_i+K}{C_i+2\Gamma^*}\sqrt{1-\left[\frac{4c(C_i+2\Gamma^*)}{C_i-\Gamma^*}\right]^{\frac{2}{3}}} \quad (13)$$

For the seasonally-fixed V_{cmax}^{25C} ($V_{cmax\_PFT}^{25C}$) and phenology-based V_{cmax}^{25C} ($V_{cmax\_LAI}^{25C}$), they are derived for the top leaves. When calculating $V_{cmax\_EEO}^{25C}$, we assume a fraction of 1 for absorbed photosynthetically active radiation to represent leaves located at the top of a canopy. This assumption ensures consistency in the derivation of canopy V_{cmax}^{25C} among the three BESS variants.

To convert top-leaf V_{cmax}^{25C} ($V_{cmax,top}^{25C}$) to representative-leaf V_{cmax}^{25C} ($V_{cmax,ave}^{25C}$), we use a satellite-based clumping index (k_n, unitless) derived from a global map[22], which indicates the non-randomness of leaf distribution[7]:

$$V_{cmax,ave}^{25C} = V_{cmax,top}^{25C} \times \frac{1 - e^{-k_n}}{k_n} \quad (14)$$

We calculate canopy-scale representative V_{cmax}^{25C} ($V_{cmax,canopy}^{25C}$) following:

$$V_{cmax,canopy}^{25C} = V_{cmax,ave}^{25C} \times LAI \quad (15)$$

Detailed deduction of V_{cmax_EEO} can be found in ref[23]. Additionally, we test the sensitivity of $V_{cmax\_EEO}^{25C}$ to the selection of the time scale for acclimation (τ) by examining its relative change when setting τ = 14 days compared to other τ values (Supplementary Fig. 9). Overall, $V_{cmax\_EEO}^{25C}$ changes by 0.17 ± 2.59 %, 0.28 ± 1.37 %, 0.14 ± 0.78 %, 0.01 ± 0.85 %, 0.37 ± 1.79 % and 1.34 ± 3.01 % (mean ± 1–SD) across flux sites when τ is set to 3, 7, 10, 20, 30 and 45 days, respectively. This finding indicates that τ has a relatively limited impact on $V_{cmax\_EEO}^{25C}$ estimation, particularly when τ is selected within the range of 7 to 30 days, a period commonly used in previous studies[23–25].

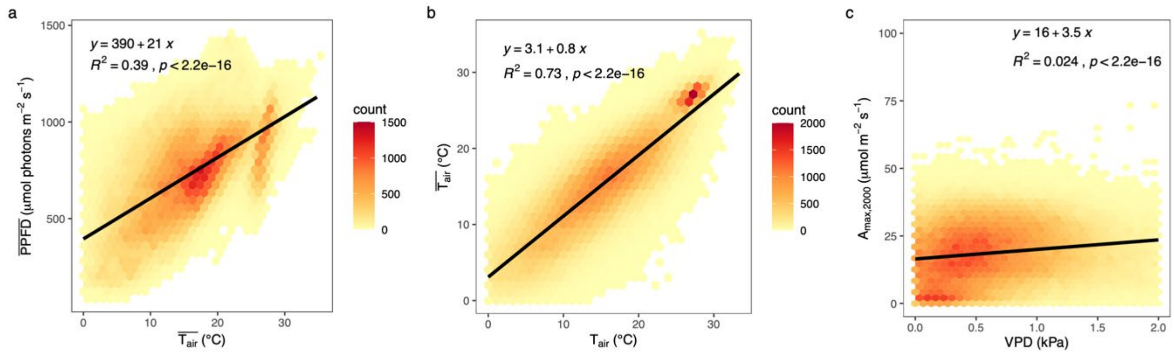

Supplementary Fig. 1: Relationships among environmental variables and $A_{max,2000}$. a–c, The relationships between $\overline{T_{air}}$ and $\overline{PPFD}$ (**a**), between $\overline{T_{air}}$ and T_{air} (**b**) and between $A_{max,2000}$ and VPD (**c**). Black lines represent linear fits (Y ~ X).

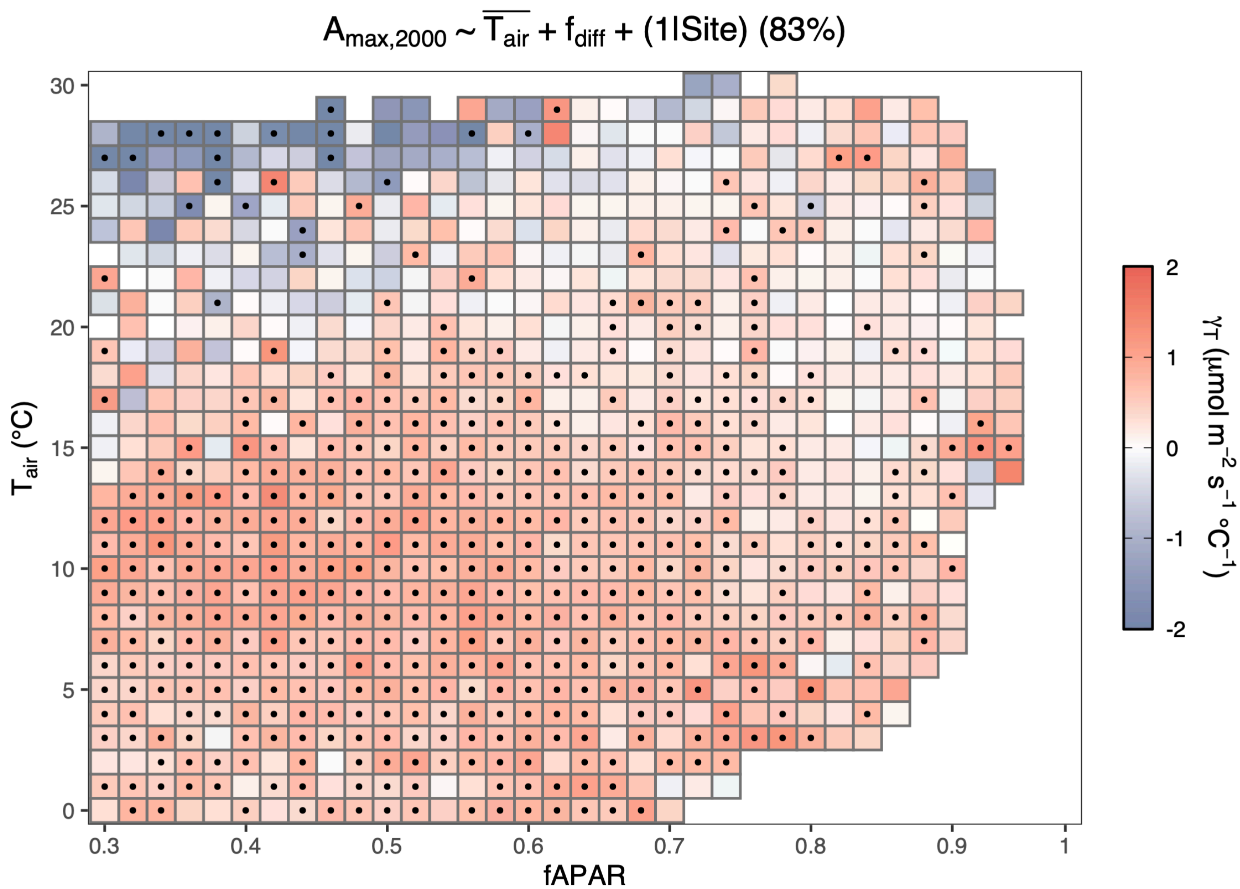

Supplementary Fig. 2: The partial effect of $\overline{T_{air}}$ on $A_{max,2000}$ over fAPAR and T_{air} bins. Diffuse fraction (f_{diff}) is incorporated in the modelling ($A_{max,2000} \sim \overline{T_{air}} + f_{diff} + (1 | Site)$). Site-level f_{diff} is estimated by an artificial neural network model[26], due to limited data availability of observed f_{diff}. Numbers (%) in parentheses represent the detectability of positive partial correlation coefficients, which is defined as the percentage of the number of bins displaying a positive partial correlation coefficient over the total number of bins. Black dots indicate significant (two-sided, $P < 0.05$) correlations.

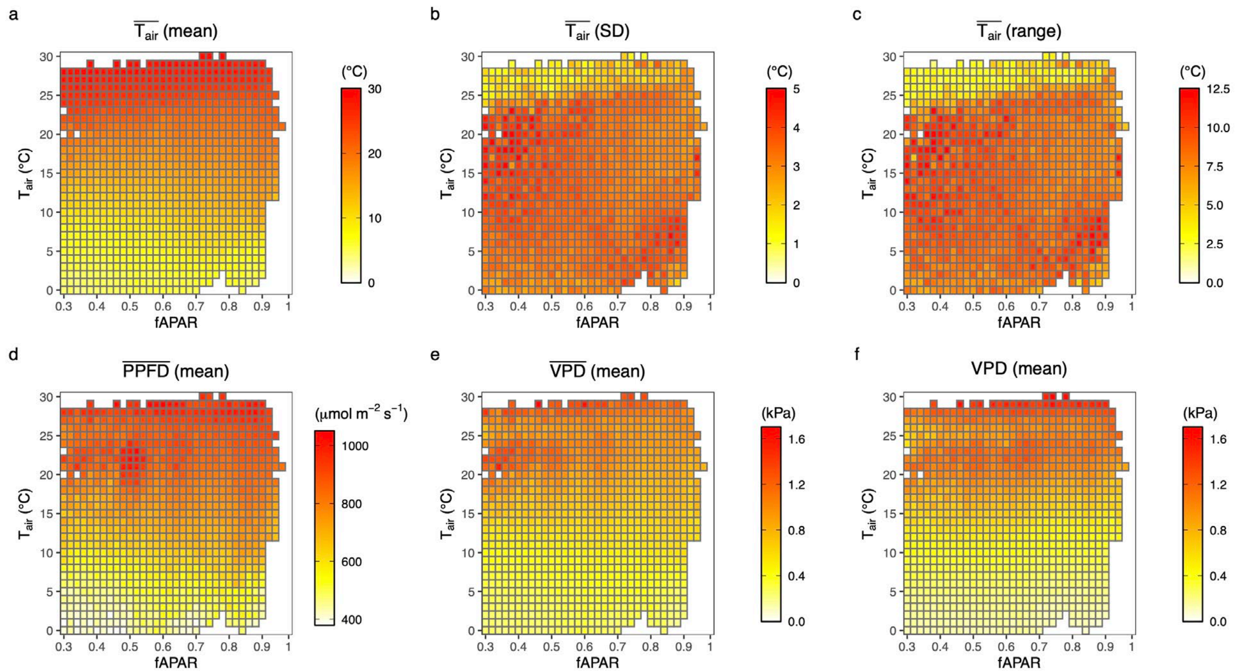

Supplementary Fig. 3: Averages (mean), standard deviations (SD) and ranges of environmental variables in the fPAR-T_{air} bin pairs for the cross-site analysis. a–c, The mean (**a**),SD (**b**) and range (**c**) of $\overline{T_{air}}$ (°C), **d,** the mean of $\overline{PPFD}$ (µmol m^{-2} s^{-1}), and **e–f,** the mean of $\overline{VPD}$ (kPa) and VPD (kPa) in each fPAR-T_{air} bin pair.

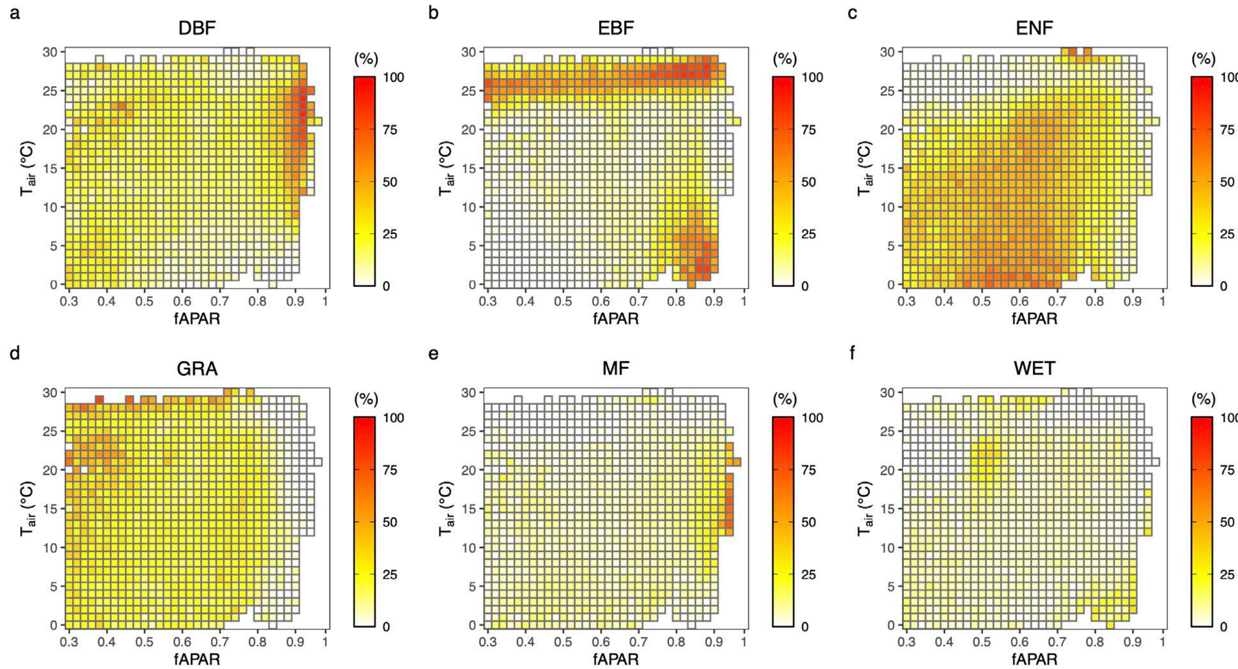

Supplementary Fig. 4: Percentage of each plant functional type (PFT) in fPAR-T_{air} bin pairs for the cross-site analysis. a–f, The ratio (%) of the number of each PFT to the total sampling number in each fPAR-T_{air} bin pair, for deciduous broadleaf forests (DBF) (**a**), evergreen broadleaf forests (EBF) (**b**), evergreen needle-leaf forests (ENF) (**c**), grasslands (GRA) (**d**), mixed forests (MF) (**e**), and wetlands (WET) (**f**).

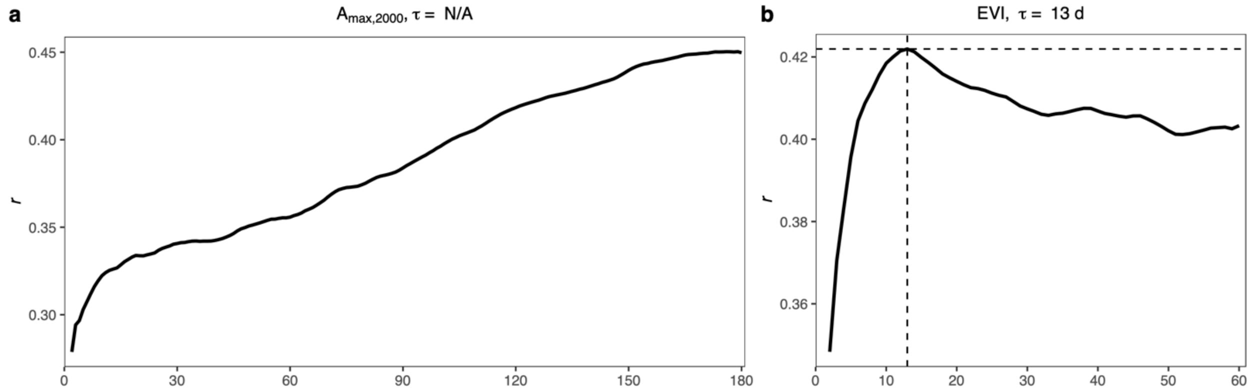

Supplementary Fig. 5: Responses of the 5-d moving average of correlation (*r*) between photosynthetic capacity metrics and $\overline{T_{air}}$ to the number of days used for averaging daytime T_{air} for evergreen broadleaf forests (EBF). a-b, $A_{max,2000}$ (**a**) and enhanced vegetation index (EVI) (**b**) are used to indicate canopy photosynthetic capacity. Daily EVI for each EBF flux site is derived from MODIS MCD43A4.

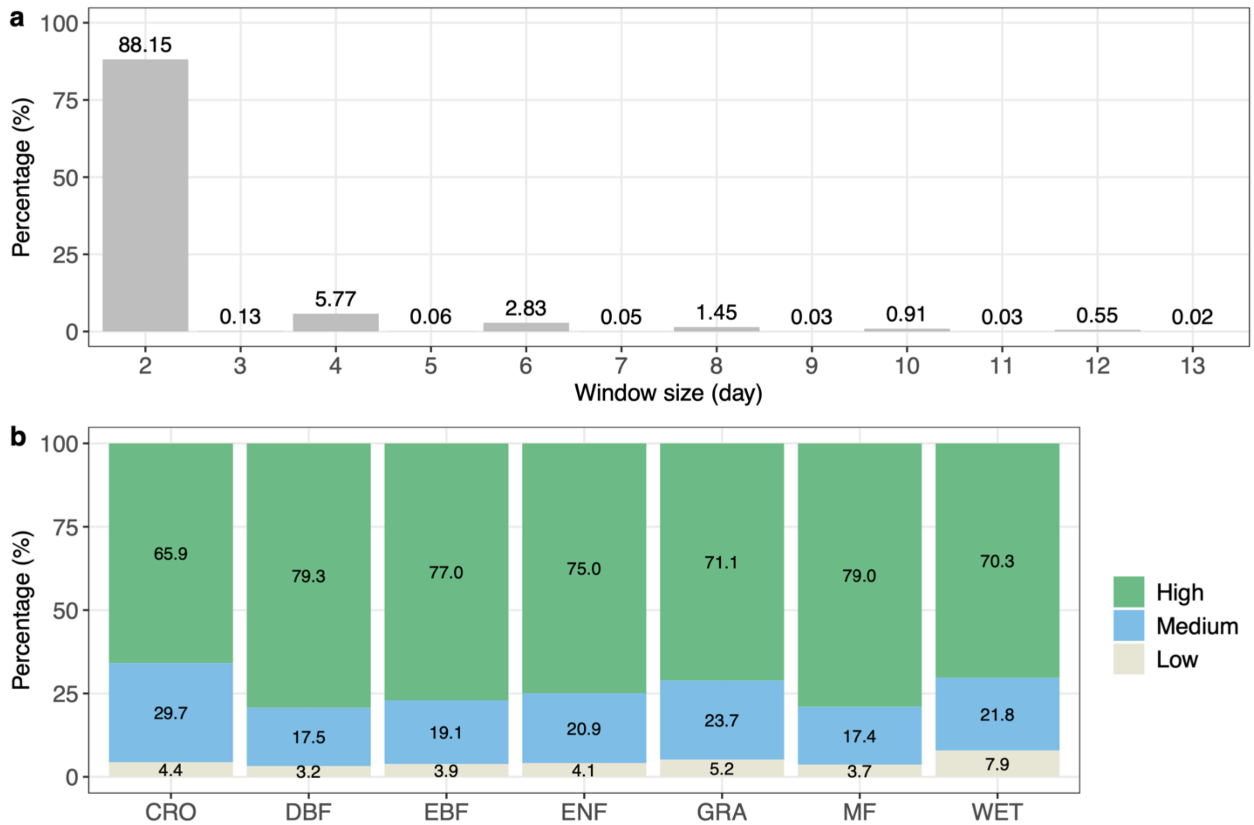

Supplementary Fig. 6: Percentages of window sizes (a) and quality flags (b) for the fitted light response curves. A "low" quality flag indicates that curve fitting cannot be well constrained with the available data within 14 days. A "medium" quality flag means the curve fitting can be constrained but the fitting parameters show unreasonable ranges. A "high" quality flag indicates that the curve fitting is well-constrained and the fitting parameters are within reasonable ranges. The reasonable range for each parameter is provided in ref.[27].

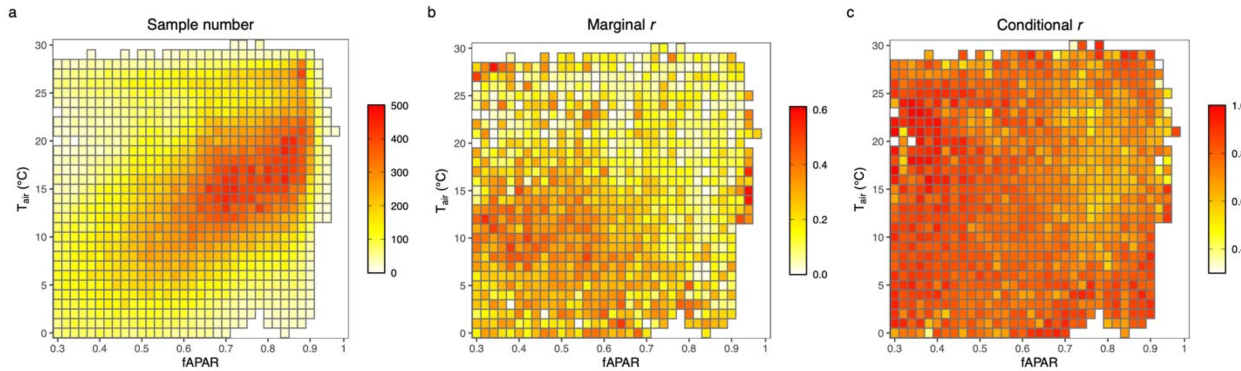

Supplementary Fig. 7: Statistical metrics for the cross-site analysis. a–c, The sampling number (**a**), marginal correlation coefficient (marginal *r*) (**b**), and conditional correlation coefficient (conditional *r*) (**c**) for the cross-site analysis using linear mix-effect models ($A_{max,2000} \sim \overline{T_{air}} + (1 \mid \text{Site})$).

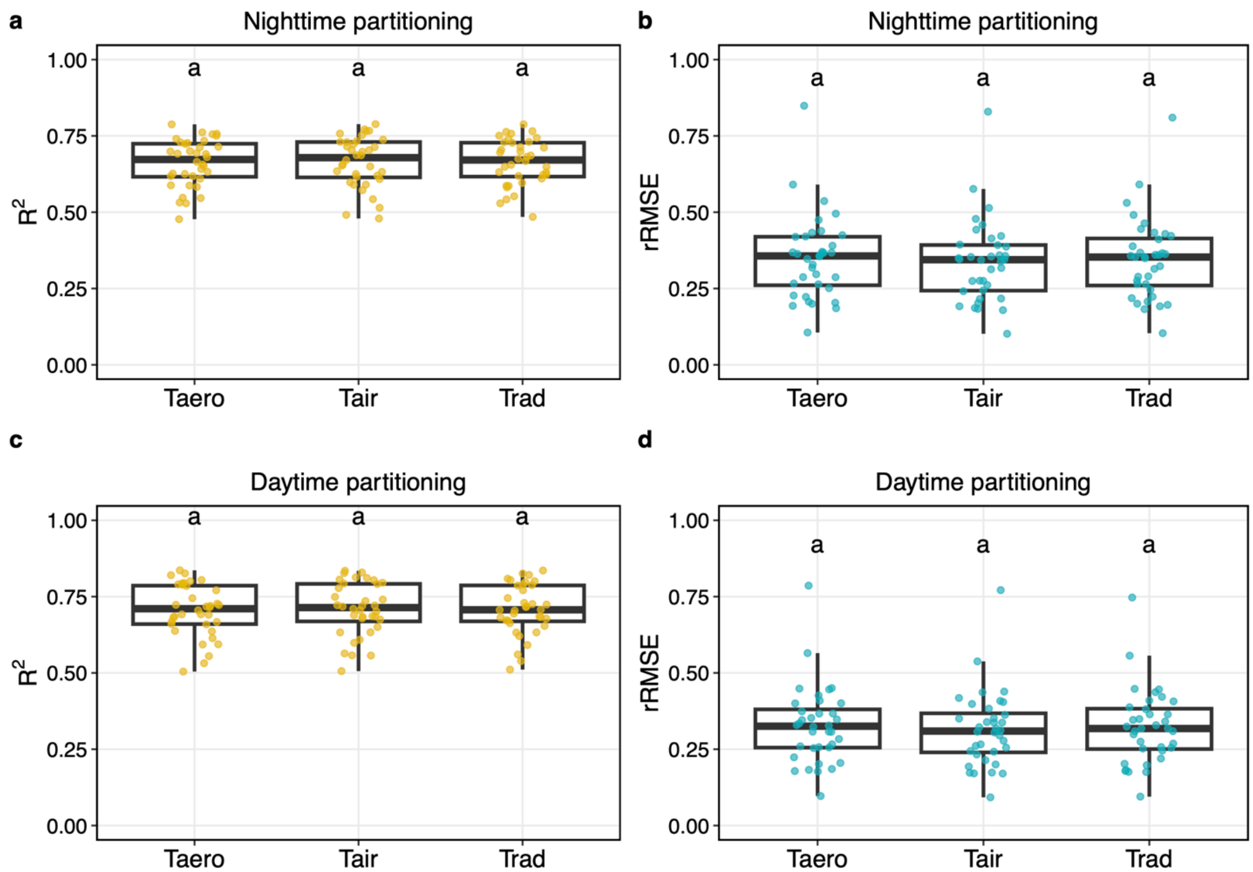

Supplementary Fig. 8: Comparison of model performance in estimating hourly GPP using three temperature approximations. a–d, Model performance is evaluated based on the coefficient of determination (R^2, golden yellow) and GPP partitioned by the nighttime (**a**) and daytime (**c**) methods, as well as relative root mean square error (rRMSE, teal) and GPP partitioned by the nighttime (**b**) and daytime (**d**) methods. The temperature approximations include aerodynamic surface temperature (T_{aero}), air temperature (T_{air}), and radiometric surface temperature (T_{rad}). In the box plots, the central lines represent the median values, the upper and lower box limits represent the 75th and 25th percentiles, and the upper and lower whiskers extend to 1.5 times the interquartile range, respectively. Identical letters indicate no statistically significant differences between the average values of the metrics, according to Tukey's HSD test (two-sided, $P > 0.05$). The analysis includes only non-cropland, non-dryland, C_3 sites with acceptable performance (see Supplementary Table 2) and with available data for incoming and outgoing longwave radiation needed for T_{rad} calculations (n = 36).

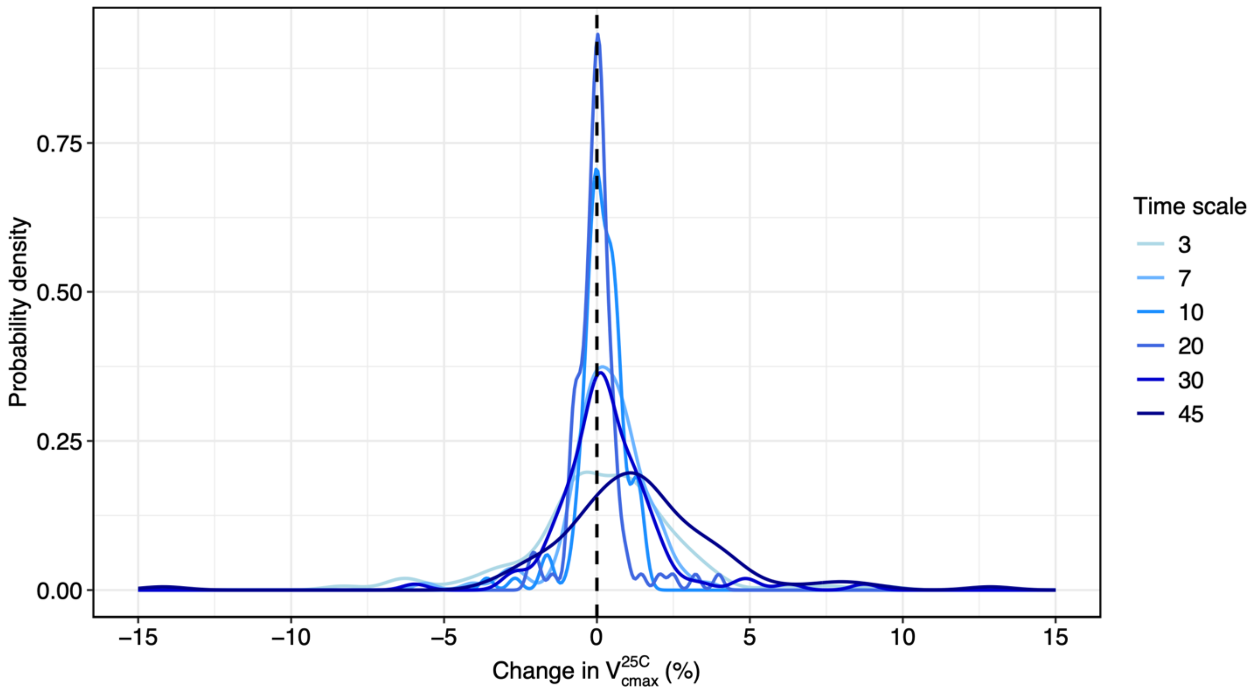

Supplementary Fig. 9: Relative change in $V_{cmax\_EEO}^{25C}$ estimated using a 14-day time scale for acclimation compared to other time scales. The probability density function for the relative change in $V_{cmax\_EEO}^{25C}$ is estimated using kernel density estimation, based on data from 105 long-term (observational length greater than three years), non-cropland, and C_3 sites.

Supplementary Table 1: Relationships between the site-level observed diffuse fraction and $\overline{T_{air}}$ for the flux sites where diffuse PAR and direct PAR are available. The diffuse fraction is calculated as the ratio of diffuse PAR to the sum of diffuse and direct PAR. The relationship between the diffuse fraction and $\overline{T_{air}}$ is modelled as a linear function (diffuse fraction ~ $\overline{T_{air}}$). Diffuse fraction and $\overline{T_{air}}$ show a significant positive relationship at only one of the 41 sites.

Site	IGBP[a]	slope	R^2	p-value
AT-Neu	GRA	-0.0033	0.0295	< 0.05
BE-Bra	MF	-0.0031	0.0293	< 0.05
CA-Gro	MF	-0.0022	0.0198	< 0.05
CA-Obs	ENF	8.00E-04	0.0029	< 0.05
CA-Qfo	ENF	-0.0013	0.0062	< 0.05
CG-Tch	SAV	-0.0242	0.1631	< 0.05
CH-Oe1	GRA	-6.00E-04	0.001	> 0.05
CH-Oe2	CRO	3.00E-04	3.00E-04	> 0.05
CZ-BK1	ENF	-0.0029	0.016	< 0.05
CZ-BK2	GRA	-0.0042	0.0139	> 0.05
DE-Geb	CRO	-0.0065	0.0869	< 0.05
DE-Hai	DBF	-0.0085	0.1278	< 0.05
DE-Tha	ENF	-0.003	0.0455	< 0.05
ES-Ln2	OSH	1.00E-04	0.003	> 0.05
FI-Hyy	ENF	-0.0017	0.0129	< 0.05
FI-Lom	WET	-0.3004	0.0167	< 0.05
FR-Gri	CRO	-0.005	0.0938	< 0.05
FR-LBr	ENF	-0.0036	0.0416	< 0.05
FR-Pue	EBF	-0.0045	0.0568	< 0.05
GF-Guy	EBF	-0.0622	0.1985	< 0.05
GH-Ank	EBF	-0.0237	0.318	< 0.05
IT-BCi	CRO	-0.0073	0.1796	< 0.05
IT-Col	DBF	-0.0055	0.0817	< 0.05
IT-MBo	GRA	-0.0019	0.0076	< 0.05
IT-PT1	DBF	0.0064	0.0126	> 0.05
IT-Ro2	DBF	-0.0068	0.1393	< 0.05
IT-SR2	ENF	-0.008	0.1565	< 0.05
IT-SRo	ENF	-0.0055	0.1152	< 0.05
NL-Loo	ENF	-0.0046	0.0915	< 0.05
RU-Ha1	GRA	-0.008	0.2058	< 0.05
US-Me1	ENF	-0.0046	0.0407	< 0.05
US-Me2	ENF	-0.0064	0.0938	< 0.05
US-MMS	DBF	-0.0027	0.0375	< 0.05
US-Ne1	CRO	-0.0023	0.0341	< 0.05
US-Ne2	CRO	-0.0017	0.0193	< 0.05
US-Ne3	CRO	-0.0019	0.024	< 0.05
US-Syv	MF	-0.0037	0.055	< 0.05
US-UMB	DBF	-0.0042	0.075	< 0.05
US-UMd	DBF	-0.0031	0.0415	< 0.05
US-Var	GRA	-0.0069	0.1031	< 0.05
US-WCr	DBF	8.00E-04	0.001	> 0.05

[a]The land cover classification defined by The International Geosphere–Biosphere Programme (IGBP) (definitions are as in Fig. 2)

Supplementary Table 2: Site information of the FLUXNET2015 database

Site	Latitude	Longitude	IGBP[a]	Period	Model[b]	DOI
AR-SLu	-33.4648	-66.4598	MF	2009-2011	No	10.18140/FLX/1440191
AR-Vir	-28.2395	-56.1886	ENF	2009-2012	No	10.18140/FLX/1440192
AT-Neu	47.11667	11.3175	GRA	2002-2012	Yes	10.18140/FLX/1440121
AU-Ade	-13.0769	131.1178	WSA	2007-2009	No	10.18140/FLX/1440193
AU-ASM	-22.283	133.249	SAV	2010-2014	No	10.18140/FLX/1440194
AU-Cpr	-34.0021	140.5891	SAV	2010-2014	No	10.18140/FLX/1440195
AU-Cum	-33.61518	150.72362	EBF	2012-2014	No	10.18140/FLX/1440196
AU-DaP	-14.0633	131.3181	GRA	2007-2013	Yes	10.18140/FLX/1440123
AU-DaS	-14.1593	131.3881	SAV	2008-2014	No	10.18140/FLX/1440122
AU-Dry	-15.2588	132.3706	SAV	2008-2014	No	10.18140/FLX/1440197
AU-Emr	-23.8587	148.4746	GRA	2011-2013	No	10.18140/FLX/1440198
AU-Fog	-12.5452	131.3072	WET	2006-2008	No	10.18140/FLX/1440124
AU-Gin	-31.3764	115.7138	WSA	2011-2014	No	10.18140/FLX/1440199
AU-GWW	-30.1913	120.6541	SAV	2013-2014	No	10.18140/FLX/1440200
AU-How	-12.4943	131.1523	WSA	2001-2014	No	10.18140/FLX/1440125
AU-Lox	-34.4704	140.6551	DBF	2008-2009	Yes	10.18140/FLX/1440247
AU-RDF	-14.5636	132.4776	WSA	2011-2013	No	10.18140/FLX/1440201
AU-Rig	-36.6499	145.5759	GRA	2011-2014	Yes	10.18140/FLX/1440202
AU-Rob	-17.1175	145.6301	EBF	2014-2014	No	10.18140/FLX/1440203
AU-Stp	-17.1507	133.3502	GRA	2008-2014	No	10.18140/FLX/1440204
AU-TTE	-22.287	133.64	GRA	2012-2014	No	10.18140/FLX/1440205
AU-Tum	-35.6566	148.1517	EBF	2001-2014	No	10.18140/FLX/1440126
AU-Wac	-37.4259	145.1878	EBF	2005-2008	No	10.18140/FLX/1440127
AU-Whr	-36.6732	145.0294	EBF	2011-2014	No	10.18140/FLX/1440206
AU-Wom	-37.4222	144.0944	EBF	2010-2014	No	10.18140/FLX/1440207
AU-Ync	-34.9893	146.2907	GRA	2012-2014	Yes	10.18140/FLX/1440208
BE-Bra	51.30761	4.51984	MF	1996-2014	No	10.18140/FLX/1440128
BE-Lon	50.55162	4.74623	CRO	2004-2014	No	10.18140/FLX/1440129
BE-Vie	50.30493	5.99812	MF	1996-2014	No	10.18140/FLX/1440130
BR-Sa1	-2.85667	-54.95889	EBF	2002-2011	No	10.18140/FLX/1440032
BR-Sa3	-3.01803	-54.97144	EBF	2000-2004	No	10.18140/FLX/1440033
CA-Gro	48.2167	-82.1556	MF	2003-2014	Yes	10.18140/FLX/1440034
CA-Man	55.87962	-98.48081	ENF	1994-2008	No	10.18140/FLX/1440035
CA-NS1	55.87917	-98.48389	ENF	2001-2005	Yes	10.18140/FLX/1440036
CA-NS2	55.90583	-98.52472	ENF	2001-2005	Yes	10.18140/FLX/1440037
CA-NS3	55.91167	-98.38222	ENF	2001-2005	Yes	10.18140/FLX/1440038
CA-NS4	55.91437	-98.380645	ENF	2002-2005	Yes	10.18140/FLX/1440039
CA-NS5	55.86306	-98.485	ENF	2001-2005	Yes	10.18140/FLX/1440040
CA-NS6	55.91667	-98.96444	OSH	2001-2005	No	10.18140/FLX/1440041
CA-NS7	56.63583	-99.94833	OSH	2002-2005	No	10.18140/FLX/1440042
CA-Oas	53.62889	-106.19779	DBF	1996-2010	Yes	10.18140/FLX/1440043
CA-Obs	53.98717	-105.11779	ENF	1997-2010	Yes	10.18140/FLX/1440044
CA-Qfo	49.6925	-74.34206	ENF	2003-2010	Yes	10.18140/FLX/1440045
CA-SF1	54.48503	-105.81757	ENF	2003-2006	No	10.18140/FLX/1440046
CA-SF2	54.25392	-105.8775	ENF	2001-2005	Yes	10.18140/FLX/1440047
CA-SF3	54.09156	-106.00526	OSH	2001-2006	No	10.18140/FLX/1440048
CA-TP1	42.6609361	-80.559519	ENF	2002-2014	No	10.18140/FLX/1440050
CA-TP2	42.7744194	-80.458775	ENF	2002-2007	No	10.18140/FLX/1440051
CA-TP3	42.7068111	-80.348314	ENF	2002-2014	No	10.18140/FLX/1440052
CA-TP4	42.710161	-80.357376	ENF	2002-2014	Yes	10.18140/FLX/1440053
CA-TPD	42.635328	-80.557731	DBF	2012-2014	Yes	10.18140/FLX/1440112
CG-Tch	-4.28917	11.65642	SAV	2006-2009	No	10.18140/FLX/1440142
CH-Cha	47.21022	8.41044	GRA	2005-2014	No	10.18140/FLX/1440131
CH-Dav	46.81533	9.85591	ENF	1997-2014	No	10.18140/FLX/1440132

CH-Fru	47.11583	8.53778	GRA	2005-2014	No	10.18140/FLX/1440133
CH-Lae	47.47833	8.36439	MF	2004-2014	No	10.18140/FLX/1440134
CH-Oe1	47.28583	7.73194	GRA	2002-2008	No	10.18140/FLX/1440135
CH-Oe2	47.28642	7.73375	CRO	2004-2014	No	10.18140/FLX/1440136
CN-Cha	42.4025	128.0958	MF	2003-2005	No	10.18140/FLX/1440137
CN-Cng	44.5934	123.5092	GRA	2007-2010	Yes	10.18140/FLX/1440209
CN-Dan	30.4978	91.0664	GRA	2004-2005	No	10.18140/FLX/1440138
CN-Din	23.1733	112.5361	EBF	2003-2005	No	10.18140/FLX/1440139
CN-Du2	42.0467	116.2836	GRA	2006-2008	Yes	10.18140/FLX/1440140
CN-Du3	42.0551	116.2809	GRA	2009-2010	Yes	10.18140/FLX/1440210
CN-Ha2	37.6086	101.3269	WET	2003-2005	No	10.18140/FLX/1440211
CN-HaM	37.37	101.18	GRA	2002-2004	Yes	10.18140/FLX/1440190
CN-Qia	26.7414	115.0581	ENF	2003-2005	No	10.18140/FLX/1440141
CN-Sw2	41.7902	111.8971	GRA	2010-2012	No	10.18140/FLX/1440212
CZ-BK1	49.50208	18.53688	ENF	2004-2014	No	10.18140/FLX/1440143
CZ-BK2	49.49443	18.54285	GRA	2004-2012	No	10.18140/FLX/1440144
CZ-wet	49.02465	14.77035	WET	2006-2014	Yes	10.18140/FLX/1440145
DE-Akm	53.86617	13.68342	WET	2009-2014	No	10.18140/FLX/1440213
DE-Geb	51.09973	10.91463	CRO	2001-2014	No	10.18140/FLX/1440146
DE-Gri	50.95004	13.51259	GRA	2004-2014	No	10.18140/FLX/1440147
DE-Hai	51.07921	10.45217	DBF	2000-2012	Yes	10.18140/FLX/1440148
DE-Kli	50.89306	13.52238	CRO	2004-2014	No	10.18140/FLX/1440149
DE-Lkb	49.09962	13.30467	ENF	2009-2013	No	10.18140/FLX/1440214
DE-Lnf	51.32822	10.3678	DBF	2002-2012	Yes	10.18140/FLX/1440150
DE-Obe	50.78666	13.72129	ENF	2008-2014	No	10.18140/FLX/1440151
DE-RuR	50.62191	6.30413	GRA	2011-2014	No	10.18140/FLX/1440215
DE-RuS	50.86591	6.44714	CRO	2011-2014	No	10.18140/FLX/1440216
DE-Seh	50.87062	6.44965	CRO	2007-2010	No	10.18140/FLX/1440217
DE-SfN	47.80639	11.3275	WET	2012-2014	Yes	10.18140/FLX/1440219
DE-Spw	51.89225	14.03369	WET	2010-2014	Yes	10.18140/FLX/1440220
DE-Tha	50.96256	13.56515	ENF	1996-2014	Yes	10.18140/FLX/1440152
DE-Zrk	53.87594	12.88901	WET	2013-2014	Yes	10.18140/FLX/1440221
DK-Eng	55.69053	12.19175	GRA	2005-2008	No	10.18140/FLX/1440153
DK-Fou	56.4842	9.58722	CRO	2005-2005	No	10.18140/FLX/1440154
DK-Sor	55.48587	11.64464	DBF	1996-2014	Yes	10.18140/FLX/1440155
ES-Amo	36.83361	-2.25232	OSH	2007-2012	No	10.18140/FLX/1440156
ES-LgS	37.09794	-2.96583	OSH	2007-2009	No	10.18140/FLX/1440225
ES-LJu	36.92659	-2.75212	OSH	2004-2013	No	10.18140/FLX/1440157
ES-Ln2	36.9695	-3.47582	OSH	2009-2009	No	10.18140/FLX/1440226
FI-Hyy	61.84741	24.29477	ENF	1996-2014	Yes	10.18140/FLX/1440158
FI-Jok	60.8986	23.51345	CRO	2000-2003	No	10.18140/FLX/1440159
FI-Let	60.64183	23.95952	ENF	2009-2012	Yes	10.18140/FLX/1440227
FI-Lom	67.99724	24.20918	WET	2007-2009	Yes	10.18140/FLX/1440228
FI-Sod	67.36239	26.63859	ENF	2001-2014	Yes	10.18140/FLX/1440160
FR-Fon	48.47636	2.7801	DBF	2005-2014	Yes	10.18140/FLX/1440161
FR-Gri	48.84422	1.95191	CRO	2004-2014	No	10.18140/FLX/1440162
FR-LBr	44.71711	-0.7693	ENF	1996-2008	No	10.18140/FLX/1440163
FR-Pue	43.7413	3.5957	EBF	2000-2014	No	10.18140/FLX/1440164
GF-Guy	5.27877	-52.92486	EBF	2004-2014	No	10.18140/FLX/1440165
GH-Ank	5.26854	-2.69421	EBF	2011-2014	No	10.18140/FLX/1440229
GL-NuF	64.13083	-51.38611	WET	2008-2014	No	10.18140/FLX/1440222
GL-ZaF	74.48143	-20.55452	WET	2008-2011	No	10.18140/FLX/1440223
GL-ZaH	74.47328	-20.5503	GRA	2000-2014	No	10.18140/FLX/1440224
IT-BCi	40.52375	14.95744	CRO	2004-2014	No	10.18140/FLX/1440166
IT-CA1	42.38041	12.02656	DBF	2011-2014	No	10.18140/FLX/1440230
IT-CA2	42.37722	12.02604	CRO	2011-2014	No	10.18140/FLX/1440231

IT-CA3	42.38	12.0222	DBF	2011-2014	No	10.18140/FLX/1440232
IT-Col	41.84936	13.58814	DBF	1996-2014	Yes	10.18140/FLX/1440167
IT-Cp2	41.70427	12.35729	EBF	2012-2014	No	10.18140/FLX/1440233
IT-Cpz	41.70525	12.37611	EBF	1997-2009	No	10.18140/FLX/1440168
IT-Isp	45.81264	8.63358	DBF	2013-2014	Yes	10.18140/FLX/1440234
IT-La2	45.9542	11.2853	ENF	2000-2002	No	10.18140/FLX/1440235
IT-Lav	45.9562	11.28132	ENF	2003-2014	No	10.18140/FLX/1440169
IT-MBo	46.01468	11.04583	GRA	2003-2013	Yes	10.18140/FLX/1440170
IT-Noe	40.60618	8.15169	CSH	2004-2014	No	10.18140/FLX/1440171
IT-PT1	45.20087	9.06104	DBF	2002-2004	Yes	10.18140/FLX/1440172
IT-Ren	46.58686	11.43369	ENF	1998-2013	No	10.18140/FLX/1440173
IT-Ro1	42.40812	11.93001	DBF	2000-2008	Yes	10.18140/FLX/1440174
IT-Ro2	42.39026	11.92093	DBF	2002-2012	No	10.18140/FLX/1440175
IT-SR2	43.73202	10.29091	ENF	2013-2014	No	10.18140/FLX/1440236
IT-SRo	43.72786	10.28444	ENF	1999-2012	No	10.18140/FLX/1440176
IT-Tor	45.84444	7.57806	GRA	2008-2014	Yes	10.18140/FLX/1440237
JP-MBF	44.3869	142.3186	DBF	2003-2005	Yes	10.18140/FLX/1440238
JP-SMF	35.2617	137.0788	MF	2002-2006	No	10.18140/FLX/1440239
MY-PSO	2.973	102.3062	EBF	2003-2009	No	10.18140/FLX/1440240
NL-Hor	52.24035	5.0713	GRA	2004-2011	Yes	10.18140/FLX/1440177
NL-Loo	52.16658	5.74356	ENF	1996-2014	No	10.18140/FLX/1440178
PA-SPn	9.31814	-79.6346	DBF	2007-2009	No	10.18140/FLX/1440180
PA-SPs	9.31378	-79.63143	GRA	2007-2009	No	10.18140/FLX/1440179
RU-Che	68.61304	161.34143	WET	2002-2005	Yes	10.18140/FLX/1440181
RU-Cok	70.82914	147.49428	OSH	2003-2014	No	10.18140/FLX/1440182
RU-Fyo	56.46153	32.92208	ENF	1998-2014	No	10.18140/FLX/1440183
RU-Ha1	54.72517	90.00215	GRA	2002-2004	Yes	10.18140/FLX/1440184
SD-Dem	13.2829	30.4783	SAV	2005-2009	No	10.18140/FLX/1440186
SJ-Adv	78.186	15.923	WET	2011-2014	No	10.18140/FLX/1440241
SJ-Blv	78.92163	11.83109	SNO	2008-2009	No	10.18140/FLX/1440242
SN-Dhr	15.40278	-15.43222	SAV	2010-2013	No	10.18140/FLX/1440246
US-AR1	36.4267	-99.42	GRA	2009-2012	No	10.18140/FLX/1440103
US-AR2	36.6358	-99.5975	GRA	2009-2012	No	10.18140/FLX/1440104
US-ARb	35.5497	-98.0402	GRA	2005-2006	Yes	10.18140/FLX/1440064
US-ARc	35.54649	-98.04	GRA	2005-2006	Yes	10.18140/FLX/1440065
US-ARM	36.6058	-97.4888	CRO	2003-2012	No	10.18140/FLX/1440066
US-Atq	70.4696	-157.4089	WET	2003-2008	No	10.18140/FLX/1440067
US-Blo	38.8953	-120.6328	ENF	1997-2007	No	10.18140/FLX/1440068
US-Cop	38.09	-109.39	GRA	2001-2007	No	10.18140/FLX/1440100
US-CRT	41.628495	-83.347086	CRO	2011-2013	No	10.18140/FLX/1440117
US-GBT	41.36579	-106.2397	ENF	1999-2006	Yes	10.18140/FLX/1440118
US-GLE	41.36653	-106.2399	ENF	2004-2014	Yes	10.18140/FLX/1440069
US-Goo	34.2547	-89.8735	GRA	2002-2006	No	10.18140/FLX/1440070
US-Ha1	42.5378	-72.1715	DBF	1991-2012	Yes	10.18140/FLX/1440071
US-IB2	41.84062	-88.24103	GRA	2004-2011	Yes	10.18140/FLX/1440072
US-Ivo	68.4865	-155.7503	WET	2004-2007	Yes	10.18140/FLX/1440073
US-KS1	28.4583	-80.6709	ENF	2002-2002	No	10.18140/FLX/1440074
US-KS2	28.6086	-80.6715	CSH	2003-2006	No	10.18140/FLX/1440075
US-Lin	36.3566	-119.8423	CRO	2009-2010	No	10.18140/FLX/1440107
US-Los	46.0827	-89.9792	WET	2000-2014	Yes	10.18140/FLX/1440076
US-LWW	34.9604	-97.9789	GRA	1997-1998	No	10.18140/FLX/1440077
US-Me1	44.5794	-121.5	ENF	2004-2005	No	10.18140/FLX/1440078
US-Me2	44.4523	-121.5574	ENF	2002-2014	No	10.18140/FLX/1440079
US-Me3	44.3154	-121.6078	ENF	2004-2009	No	10.18140/FLX/1440080
US-Me4	44.4992	-121.6224	ENF	1996-2000	No	10.18140/FLX/1440081
US-Me5	44.43719	-121.56676	ENF	2000-2002	No	10.18140/FLX/1440082

US-Me6	44.3232842	-121.6078	ENF	2010-2014	No	10.18140/FLX/1440099
US-MMS	39.3232	-86.4131	DBF	1999-2014	Yes	10.18140/FLX/1440083
US-Myb	38.049861	-121.76498	WET	2010-2014	No	10.18140/FLX/1440105
US-Ne1	41.16506	-96.47664	CRO	2001-2013	No	10.18140/FLX/1440084
US-Ne2	41.16487	-96.4701	CRO	2001-2013	No	10.18140/FLX/1440085
US-Ne3	41.17967	-96.43965	CRO	2001-2013	No	10.18140/FLX/1440086
US-NR1	40.0329	-105.5464	ENF	1998-2014	Yes	10.18140/FLX/1440087
US-Oho	41.5545	-83.8438	DBF	2004-2013	Yes	10.18140/FLX/1440088
US-ORv	40.0201	-83.0183	WET	2011-2011	No	10.18140/FLX/1440102
US-PFa	45.9459	-90.2723	MF	1995-2014	No	10.18140/FLX/1440089
US-Prr	65.12367	-147.48756	ENF	2010-2014	Yes	10.18140/FLX/1440113
US-SRC	31.9083	-110.8395	MF	2008-2014	No	10.18140/FLX/1440098
US-SRG	31.789379	-110.82768	GRA	2008-2014	No	10.18140/FLX/1440114
US-SRM	31.8214	-110.8661	WSA	2004-2014	No	10.18140/FLX/1440090
US-Sta	41.3966	-106.8024	OSH	2005-2009	No	10.18140/FLX/1440115
US-Syv	46.242	-89.3477	MF	2001-2014	No	10.18140/FLX/1440091
US-Ton	38.4316	-120.96598	WSA	2001-2014	No	10.18140/FLX/1440092
US-Tw1	38.1074	-121.6469	WET	2012-2014	No	10.18140/FLX/1440108
US-Tw2	38.1047	-121.6433	CRO	2012-2013	No	10.18140/FLX/1440109
US-Tw3	38.1159	-121.6467	CRO	2013-2014	No	10.18140/FLX/1440110
US-Tw4	38.10298	-121.6414	WET	2013-2014	No	10.18140/FLX/1440111
US-Twt	38.1087204	-121.6531	CRO	2009-2014	No	10.18140/FLX/1440106
US-UMB	45.5598	-84.7138	DBF	2000-2014	Yes	10.18140/FLX/1440093
US-UMd	45.5625	-84.6975	DBF	2007-2014	Yes	10.18140/FLX/1440101
US-Var	38.4133	-120.9507	GRA	2000-2014	Yes	10.18140/FLX/1440094
US-WCr	45.8059	-90.0799	DBF	1999-2014	Yes	10.18140/FLX/1440095
US-Whs	31.7438	-110.0522	OSH	2007-2014	No	10.18140/FLX/1440097
US-Wi0	46.618778	-91.081444	ENF	2002-2002	Yes	10.18140/FLX/1440055
US-Wi1	46.730472	-91.232944	DBF	2003-2003	Yes	10.18140/FLX/1440054
US-Wi2	46.686889	-91.152833	ENF	2003-2003	No	10.18140/FLX/1440056
US-Wi3	46.634722	-91.098667	DBF	2002-2004	Yes	10.18140/FLX/1440057
US-Wi4	46.739333	-91.16625	ENF	2002-2005	No	10.18140/FLX/1440058
US-Wi5	46.653083	-91.085806	ENF	2004-2004	Yes	10.18140/FLX/1440059
US-Wi6	46.624889	-91.298222	OSH	2002-2003	No	10.18140/FLX/1440060
US-Wi7	46.649111	-91.069278	OSH	2005-2005	No	10.18140/FLX/1440061
US-Wi8	46.722333	-91.252417	DBF	2002-2002	Yes	10.18140/FLX/1440062
US-Wi9	46.618778	-91.081444	ENF	2004-2005	No	10.18140/FLX/1440063
US-Wkg	31.7365	-109.9419	GRA	2004-2014	No	10.18140/FLX/1440096
US-WPT	41.464639	-82.996157	WET	2011-2013	No	10.18140/FLX/1440116
ZM-Mon	-15.4391	23.2525	DBF	2000-2009	No	10.18140/FLX/1440189

[a]The land cover classification defined by The International Geosphere–Biosphere Programme (IGBP) (definitions are as in Fig. 1)

[b]If the site is C_3, non-cropland and non-dryland, and demonstrates acceptable model performance ($R^2 > 0.5$) across all three model variants

Supplementary Table 3: Parameter values for temperature dependency functions of V_{cmax} and J_{max} (equation 5)

Parameters	$H_{a,v}$[a]	$H_{a,j}$[b]	S_v[c]	S_j[d]	b_{jv}[e]
a	1.14	0	-0.38	0	0
b	0	0	0	-0.84	-0.0375
c	0	0	0	-0.52	-0.0202
d	42.6	40.71	645.13	658.77	2.56

[a]Activation energy of V_{cmax}

[b]Activation energy of J_{max}

[c]Entropy term of V_{cmax}

[d]Entropy term of J_{max}

[e]The ratio of J_{max}^{25C} to V_{cmax}^{25C}

References

1. Farquhar, G. D., von Caemmerer, S. & Berry, J. A. A biochemical model of photosynthetic CO_2 assimilation in leaves of C_3 species. *Planta* **149**, 78–90 (1980).
2. Jiang, C. & Ryu, Y. Multi-scale evaluation of global gross primary productivity and evapotranspiration products derived from Breathing Earth System Simulator (BESS). *Remote Sensing of Environment* **186**, 528–547 (2016).
3. Ryu, Y. *et al.* Integration of MODIS land and atmosphere products with a coupled-process model to estimate gross primary productivity and evapotranspiration from 1 km to global scales. *Global Biogeochemical Cycles* **25**, 1–24 (2011).
4. Knauer, J., El-Madany, T. S., Zaehle, S. & Migliavacca, M. Bigleaf—An R package for the calculation of physical and physiological ecosystem properties from eddy covariance data. *PLoS ONE* **13**, 1–26 (2018).
5. Baldocchi, D. An analytical solution for coupled leaf photosynthesis and stomatal conductance models. *Tree Physiology* **14**, 1069–1079 (1994).
6. Wang, H. *et al.* Towards a universal model for carbon dioxide uptake by plants. *Nature Plants* **3**, 734–741 (2017).
7. De Pury, D. G. G. & Farquhar, G. D. Simple scaling of photosynthesis from leaves to canopies without the errors of big-leaf models. *Plant, Cell and Environment* **20**, 537–557 (1997).
8. Kumarathunge, D. P. *et al.* Acclimation and adaptation components of the temperature dependence of plant photosynthesis at the global scale. *New Phytologist* **222**, 768–784 (2019).

9. Li, B. *et al.* BESSv2.0: A satellite-based and coupled-process model for quantifying long-term global land–atmosphere fluxes. *Remote Sensing of Environment* **295**, 113696 (2023).
10. Knauer, J. *et al.* Higher global gross primary productivity under future climate with more advanced representations of photosynthesis. *Sci. Adv.* **9**, eadh9444 (2023).
11. Verma, S. B. Aerodynamic resistances to transfers of heat, mass and momentum. in *Estimation of areal evapotranspiration (pp. 13–20)* (Wallingford, UK: International Association of Hydrological Sciences IAHS Publication No. 177, 1989).
12. Thom, A. S. Momentum, mass and heat exchange of vegetation. *Q.J Royal Met. Soc.* **98**, 124–134 (1972).
13. Pastorello, G. *et al.* The FLUXNET2015 dataset and the ONEFlux processing pipeline for eddy covariance data. *Scientific Data* **7**, 225 (2020).
14. Chen, J. L., Reynolds, J. F., Harley, P. C. & Tenhunen, J. D. Coordination theory of leaf nitrogen distribution in a canopy. *Oecologia* **93**, 63–69 (1993).
15. Maire, V. *et al.* The coordination of leaf photosynthesis links C and N fluxes in C_3 plant species. *PLoS ONE* **7**, 1–15 (2012).
16. Stocker, B. D. *et al.* P-model v1.0: An optimality-based light use efficiency model for simulating ecosystem gross primary production. *Geoscientific Model Development* **13**, 1545–1581 (2020).
17. Smith, E. L. The influence of light and carbon dioxide on photosynthesis. *Journal of General Physiology* **20**, 807–830 (1937).
18. Bernacchi, C. J., Pimentel, C. & Long, S. P. *In vivo* temperature response functions of parameters required to model RuBP-limited photosynthesis: Modelling RuBP-limited photosynthesis. *Plant, Cell & Environment* **26**, 1419–1430 (2003).

19. Prentice, I. C., Dong, N., Gleason, S. M., Maire, V. & Wright, I. J. Balancing the costs of carbon gain and water transport: Testing a new theoretical framework for plant functional ecology. *Ecology Letters* **17**, 82–91 (2014).

20. Bernacchi, C. J., Singsaas, E. L., Pimentel, C., Portis, A. R. & Long, S. P. Improved temperature response functions for models of Rubisco-limited photosynthesis. *Plant, Cell and Environment* **24**, 253–259 (2001).

21. Kattge, J. & Knorr, W. Temperature acclimation in a biochemical model of photosynthesis: A reanalysis of data from 36 species. *Plant, Cell and Environment* **30**, 1176–1190 (2007).

22. He, L., Chen, J. M., Pisek, J., Schaaf, C. B. & Strahler, A. H. Global clumping index map derived from the MODIS BRDF product. *Remote Sensing of Environment* **119**, 118–130 (2012).

23. Jiang, C., Ryu, Y., Wang, H. & Keenan, T. F. An optimality-based model explains seasonal variation in C_3 plant photosynthetic capacity. *Global Change Biology* **26**, 6493–6510 (2020).

24. Luo, X. & Keenan, T. F. Global evidence for the acclimation of ecosystem photosynthesis to light. *Nature Ecology and Evolution* **4**, 1351–1357 (2020).

25. Smith, N. G. & Dukes, J. S. Short-term acclimation to warmer temperatures accelerates leaf carbon exchange processes across plant types. *Global Change Biology* **23**, 4840–4853 (2017).

26. Zhou, H. *et al.* Large contributions of diffuse radiation to global gross primary productivity during 1981–2015. *Global Biogeochemical Cycles* **35**, e2021GB006957 (2021).

27. Lasslop, G. *et al.* Separation of net ecosystem exchange into assimilation and respiration using a light response curve approach: Critical issues and global evaluation. *Global Change Biology* **16**, 187–208 (2010).